Omnidirectional Dual-Polarized Low-Profile Textile Rectenna with over 50% Efficiency for Sub-μW/cm^2 Wearable Power Harvesting

Mahmoud Wagih, *Graduate Student Member, IEEE*, Alex S. Weddell, *Member, IEEE*, and Steve Beeby, *Senior Member, IEEE*

Abstract—Despite the recent advances in textile antennas, in complete systems such as a rectenna, the efficiency of fully-textile solutions has been over 46% lower than hybrid textile/rigid implementations. This paper presents a fully-textile rectenna for ultra-low power sub-μW/cm^2 applications. A dual-polarized omnidirectional low-profile textile antenna is presented. The rectenna is based on a compact inductively-matched rectifier. The textile-based rectifier occupies 0.22 cm^2 and achieves a state-of-art Power Conversion Efficiency (PCE) of 41.8% at -20 dBm, at 820 MHz, despite its lossy substrate. A triple-band rectifier is then designed and fabricated to show the scalability of the matching approach. The rectifier is characterized using a new figure of merit "average PCE" over a time period while charging a capacitor. Time-varying s-parameters are used to quantify the impact of the capacitor's charge on the impedance matching. The rectifier directly charges a 1.32 mF capacitor up to 1 V in 0.41 and 4.5 seconds from 10 and 0 dBm, respectively. Wireless testing of the proposed rectenna demonstrates over 50% and 40% PCE below 1 μW/cm^2 in space and on-body, respectively. The rectenna efficiently receives power from mismatched polarization and with a 360° half-power beamwidth.

Index Terms—Antenna, Electronic Textiles, Microstrip antennas, Rectenna, Radio Frequency Energy Harvesting (RFEH), Wearable Antenna, Wireless Power Transfer.

I. INTRODUCTION

TEXTILE and flexible Radio Frequency (RF) electronics and antennas are seen as an enabling technology of wearable Internet of Things (IoT) and Body Area Networks (BAN). This has led to extensive research activities on wearable antennas, both employing flexible and textile materials [1], as well as non-textile rigid substrates [2]. RF Energy Harvesting (RFEH) is seen as a method of enabling battery-free wearable electronics, benefiting from the advances in wearable RF electronics. Rectennas can be realized using standard antenna designs such as microstrip patches and bow-tie arrays using flexible and textile conductors [1], [3]–[6].

Rectennas are an example of complete systems which can be fabricated using textile materials. All-textile RF systems include both lumped devices, such as transmitters, power amplifiers or diodes, in addition to textile antennas [7]. Textile antennas have been extensively researched and have shown performance comparable to their rigid counterparts [4]. The advances in textile antennas leverage fabrication methods such as conductive fabrics [4], [8]–[11], and embroidered conductors [5], [12]. A demonstration of a functional RF textile system is presented in [7], where a power amplifier is integrated with bespoke fabric transmission lines.

The performance of a rectenna is a function of multiple parameters. First of all, the antenna's radiation efficiency, gain, polarization, and beamwidth affect the power received by the rectenna from an incident plane wave [13], [14]. A wide beamwidth is particularly crucial for harvesting ambient radiation [14], or when powering mobile wearable receivers where angular alignment between the transmitter and receiver is unlikely [15]. In addition, maintaining compactness is highly-desired for unobtrusive IoT [16]. The rectifier's RF to DC Power Conversion Efficiency (PCE) is controlled by the rectenna's source and load impedances, and is limited at low power levels by the diode's forward voltage [17]. Theoretical and experimental analysis have previously been used to evaluate the maximum-achievable PCE based on a commercial Schottky diode [18]. The rectennas reported in literature with the maximum PCE have been mostly based on antenna-rectifier co-design techniques [18], [19], or matching networks based on iterative source and load impedance tuning [4]. In a wearable rectenna, the available methods to maximizing the PCE will be limited by the fabric's dielectric properties and the conductive materials.

For flexible textile-based wearable rectennas, the textile dielectric properties ($\tan\delta$) limit the choice of impedance matching networks. A large distributed matching network will result in higher insertion losses. Although a flexible rectenna with a textile patch antenna in presented in [4], the high PCE achieved at low power levels is attributed to the rectifier's implementation on a low-loss rigid substrate. In addition, rigid RF sub-circuits interfaced with e-textiles are seen as the only method of enabling a high performance system [4], [20]. Although sub-1 GHz and a 2.4 GHz fully-textile rectennas have been presented with textile-based rectifiers [1], [5], their PCE has been lower than their counterparts with a rigid rectifier such as [4], [16]. For example, at 2.4 GHz and -20 dBm of RF power, the PCE of the textile-based rectifier in [5] was over 46% lower than that in [4] implemented on a low-loss substrate using the same diode.

The authors are with the School of Electronics and Computer Science, University of Southampton, Southampton, SO17 1BJ, U.K. (email: mahm1g15@ecs.soton.ac.uk, asw@ecs.soton.ac.uk, spb@ecs.soton.ac.uk)

In human-proximity, antennas are expected to detune resulting in significant resonance shifts [21], as well as have their radiation efficiency reduced [22]. To counter this problem in rectennas and be able to receive power efficiently, the majority of textile-based rectennas have been based on broadside off-body patch antennas [1], [4], [5]. However, patch antennas require thick substrates >2 mm to achieve high radiation efficiency [4]. Moreover, patches are inherently narrow band, limiting their application to single-tone Wireless Power Transfer (WPT). Patches also occupy larger area than monopole and dipole omnidirectional antennas. Recently, a broadband wearable rectenna has been based on un-isolated bow-tie elements [6]. The broadband design implies that an unshielded antenna is used [8]. Hence the rectenna's PCE has been over 50% lower than its textile microstrip patch counterpart in [1], at the same power density.

On the other hand, several studies have pointed out the need for un-shielded wearable antennas at sub-1 GHz bands. For instance, due to size and subsequently radiation efficiency limitation, it may not feasible to implement antennas with unconnected reflector backing at sub-1 GHz bands [23]. Furthermore, it has been shown analytically, based on real textile antennas, that the received power can be enhanced by over $10\times$ at 915 MHz using an unshielded monopole compared to a high-efficiency 2.4 GHz patch [15].

To demonstrate the feasibility of ultra low-power (<1 μW/cm^2) wireless energy harvesting for wearable applications, it is crucial to realize a fully-textile rectenna with a high PCE. For non-textile rectennas implemented on low-loss substrates, the highest reported sub-1 GHz PCE at -20 dBm of 34% has been achieved in [19], using a complex conjugate antenna with a predominately reactive rectifier. At 2.4 GHz, the highest efficiency achieved of 40% has also been achieved using a large complex-conjugate antenna on a low-loss substrates [24]. To the best of our knowledge, these are the highest PCEs using commercial Schottky diodes. Both implementations, [24] and [19], require careful antenna tuning which will significantly degrade in human proximity and are hence unsuitable for wearable applications.

This work demonstrates the feasibility of high-PCE wireless energy harvesting using low-profile, broadband, all-textile rectennas. A dual-polarization compact fully-textile broadband antenna is presented on a 1 mm felt substrate and evaluated on the body (sections II and III). The rectenna uses a compact lumped-matched rectifier achieving a best-in-class PCE of 41.8% at -20 dBm (sections IV and V). To demonstrate the scalability of the matching approach, a multi-band rectifier is designed and evaluated. Finally, time-variant s-parameter measurements are presented (section V) showing the textile-based rectifier directly charging a capacitor as well as investigating the effect of the capacitors' charge-state on the rectifier's input impedance. In wireless testing (section VI), the proposed rectenna achieves over $5\times$ higher PCE than state-of-art textile rectennas at power densities less than 1 μW/cm^2. When tested on-body, the rectenna achieves over 40% PCE from an incident 1 μW/cm^2 plane-wave. The rectenna's dual-polarization harvesting capability is demonstrated along with a 360° omnidirectional half-power beamwidth.

II. Textile Antenna Design and Fabrication

A. Fully-Textile Rectenna Fabrication Technique

Felt, a non-woven textile produced through compression and matting of fibers (typically wool), is expected to have a relative permittivity (ϵ_r) close to that of air, due to its low density and porous structure. It is expected to suffer from lower dielectric losses compared to other woven textiles due to the increased porosity reducing its loss tangent (tanδ). As a result, for textile antennas with the highest radiation efficiency felt has been used a substrate [4]. Furthermore, 1 mm felt was reported to have a minimal impact on on-body propagation at 60 GHz compared to 0.2 mm cotton, despite its higher thickness due to its mostly-air composition [25].

In order to validate the assumptions about the felt's properties and to accurately model the rectenna in 3D full-wave simulation, 1 mm-thick commercial felt has been characterized using the two-line method [26], [27]. The 1 mm felt was used as a substrate for two microstrip lines of 40 and 60 mm length and 4 mm trace width. Based on the dielectric properties reported in [4], the trace width has been selected to realize a 50Ω microstrip line. The measured dielectric properties of felt are ϵ_r=1.12 and tanδ=0.023.

In order to realize a high-efficiency antenna with minimal conductive losses due to surface roughness and resistivity, the conductor material needs to be chosen carefully. Printed antennas on textile suffer from around 10 μm surface roughness which reduces the trace conductivity at microwave bands. Copper foils, polyimide copper laminates, and metalized shielding fabrics are mechanically more reliable and resilient to cracking compared to printed traces [28]. Moreover, their sheet resistance is lower than that of low-temperature conductive silver inks [29]. As the proposed antenna features are all larger than 1 mm, laser or die-cutting can be utilized for faster turn-around and reduced fabrication costs. Conductive fabric (P&P Microwave weave, 0.005 Ω/square, with adhesive backing) was chosen as it offers improved user comfort compared to flexible copper sheets. The fabric have been cut using a standard CO_2 laser-cutter, to create features larger than 1 mm, as shown in Fig. 1-a.

To fabricate a miniaturized rectifier supporting low-footprint component packages photolithography has to be utilized. The process described in [30] and [21], previously used to realize high efficiency antennas at microwave and mmWave bands, has been utilized to fabricate the rectifier (Fig. 2-c). Features down to 150 μm, such as surface mount components pads, can be easily resolved using a commercial copper etcher and a standard UV light source without the need for a clean room environment. Textile-based electronics require encapsulation for improved reliability [31], [32]. Fabricating flexible circuits on thin polyimide filaments for textiles integration support encapsulation techniques such as vacuum-forming [32]. Encapsulated RFID tags have been demonstrated withstanding over 30 machine washing cycles [32]. Fig. 2 shows photographs of the fabricated rectenna and rectifier prototypes.

The unresolved challenge in realizing a RF textile system employing two fabrication processes is in demonstrating a low-loss transition between the transmission lines. Establishing
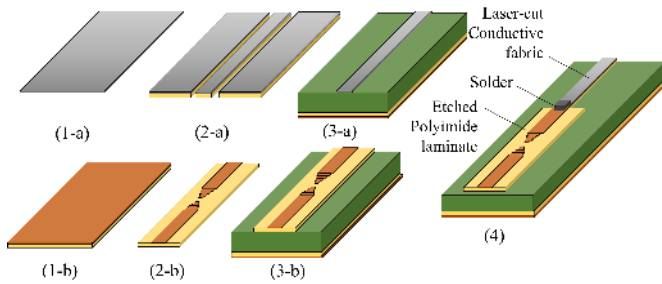
Fig. 1. Textile rectenna fabrication steps: (1-a) conductive fabric prior to cutting, (2-a) laser cut antenna traces, (3-a) adhered laser-cut traces on the felt substrate. (1-b) polyimide copper laminate, (2-b) etched copper laminates, (3-b) etched traces adhered to felt, (4) integration of laser-cut and etched Polyimide laminates using a solder interface.
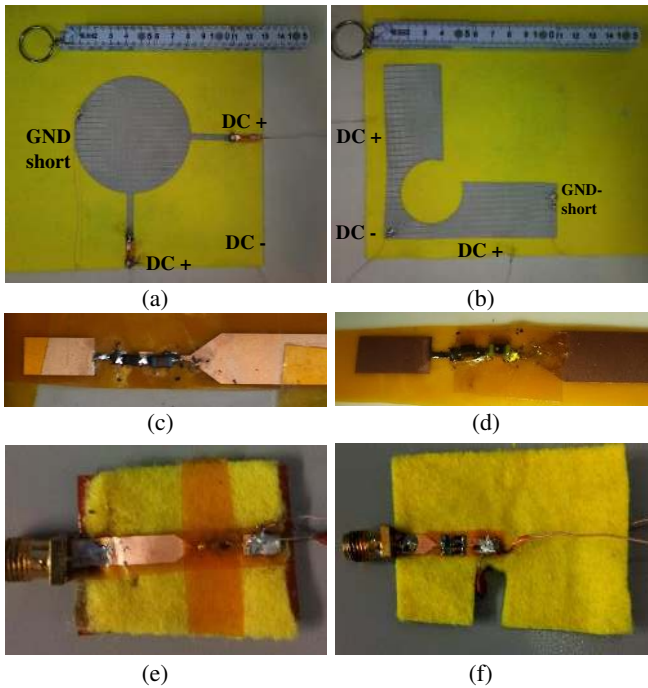

Fig. 3. The textile-flexible circuit interface measured s-parameters (left) and photograph of the 60 mm-length prototype (right).

Fig. 2. Photographs of the rectenna and rectifier prototypes: (a) top-side of the assembled rectenna, (b) bottom-side of the assembled rectenna, (c) close-up photo of the rectifier prior to integration with the textile substrate, (d) the rectifier following Kapton encapsulation, (e) the single band connectorized rectifier used in PCE measurements, (f) the multi-band rectifier prototype.

PCB transition, two 60 mm microstrip lines were fabricated, a fully flexible copper line, and a hybrid 50% copper, 50% conductive fabric with a soldered interconnect line. The insertion losses through both lines are measured using a Vector Network Analyser (VNA) up to 2 GHz. Compared to the fully copper line, as shown in Fig. 3, the hybrid line experiences only 0.50, 0.41 and 0.22 dB additional insertion losses at 0.75, 1.9, and 2.4 GHz, respectively. Therefore demonstrating the lowest loss on-fabric transition compared to [4] and [33].

B. Dual-Polarization Broadband On-Body Antenna

In recent implementations, ambient RFEH has been synonymous with multi-band harvesting [13]. To explain, in order to harvest a considerable power density from ambient sources, the antenna needs to radiate at multiple bands between 0.7 and 2.7 GHz [34]. Hence, dual [35], triple [36], [37], broadband [38], and six-band rectennas are becoming increasingly popular [39].

Broadband antennas, mainly developed for Ultra-Wide-Band (UWB) communication (3-10 GHz) [40], can be scaled to cover the UHF microwave bands of interest in RFEH context. A simple microstrip-fed design, the circular disc monopole [40], is adopted in this work, due to ease of implementation using the proposed fabrication technique. Furthermore, being a free-standing planar monopole antenna with no ground-plane-backing, the electric-fields dissipated in the lossy textile substrate will be minimized implying the possibility of achieving higher gain and radiation efficiency.

In order to efficiently harvest arbitrarily-propagating RF power, the antenna needs to be independent of the incident wave's polarization angle to avoid Polarization Mismatch Loss (PML), where angular alignment with the cellular or wireless-charging base-station is highly unlikely [13]. Dual-Linearly-Polarised (LP) has previously demonstrated angular-independence, as well as the ability to receive a Circularly Polarised (CP) wave (regardless of the direction) at both ports [41]. When the outputs are combined, this avoids the -3 dB CP to LP PML, observed when utilizing a CP rectenna to harvest LP waves [41].

The circular monopole design has been modified to include two feeding points, for horizontal and vertical LP reception. Both ports are fed using 50Ω microstrip lines for ease of

a connection between textile RF transmission lines and a standard Printed Circuit Board (PCB) has been addressed previously using broadside coupling between a fabric and a Duroid microstrip with 0.7 dB losses at 2.4 GHz [4], and hook-on flexible interconnects of approximately 1 dB loss up to 2 GHz [33]. As the thickness of the conductive fabric and the flexible Polyimide PCB is comparable, a solder interface can be utilized at the transition between the copper and conductive fabric, as shown in Fig. 1 and 3. Low-temperature solder (melting point=170°C) is utilized to prevent damaging the metalized woven threads of the antenna, alternatively, a layer of thin conductive epoxy can be used in order to further reduce process temperatures, making this transition compatible with all textile materials.

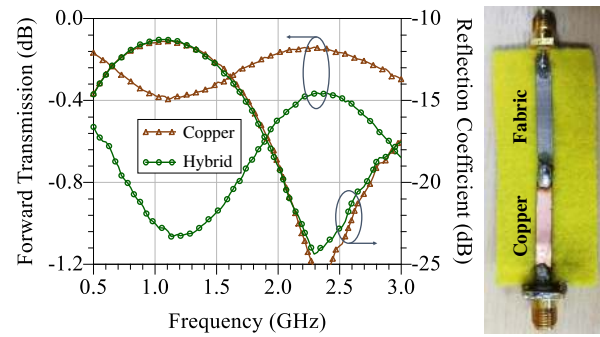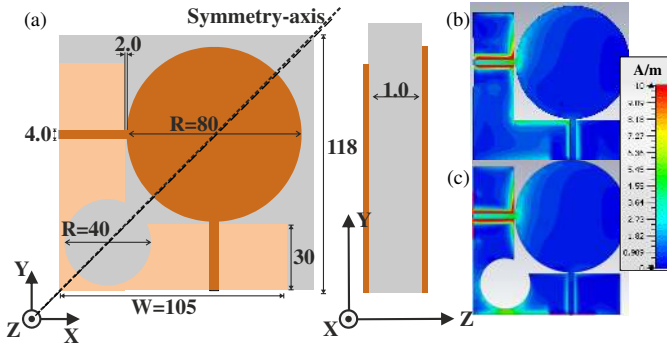To investigate the effect of the conductive fabric to flexible

Fig. 4. Dual-polarization broadband disc monopole geometry (a), dimensions in mm, and the surface current plot at 900 MHz before (b) and after (c) ground-voiding.
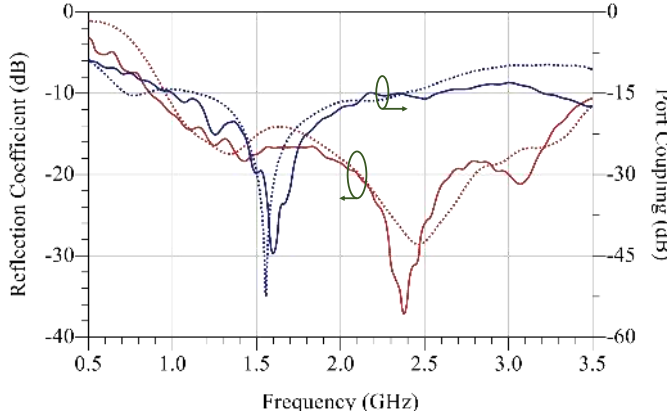

Fig. 5. Simulated (dashed) and measured (solid) reflection coefficient (S_{11}) and port coupling (S_{21}) of the proposed dual-polarization textile monopole.

testing, and for integration with 50Ω-matched rectifiers. The ground planes of both ports overlap at the corner of the antenna, increasing the antenna's port coupling (S_{21}). The simulated surface current plot of the antenna at 900 MHz, in Fig. 4, shows that a significant portion of the current travels from the H-LP port to the V-LP port through the inner corner of the ground plane. Therefore, the antenna design is modified through voiding the ground plane using a circular notch to prevent the current flow between the ports. In the CST simulations, the circular notch improves the port-isolation by 5 dB from 0.8 to 2.4 GHz. In the context of RFEH, this increases the amount of RF power at the individual port, allowing the rectifier to achieve higher PCEs.

III. ANTENNA SIMULATION AND MEASUREMENT

The antenna has been simulated using 3D full-wave simulation in CST Microwave Studio, the simulation model utilizes the extracted material properties of the substrate, as well as a lossy copper model with 1 μm surface roughness, to accurately model the skin effect losses. The s-parameters were measured using a ZVB4 VNA, Fig. 5 shows the simulated and measured s-parameters of the antenna, showing a $S_{11} < -10$ dB bandwidth from 800 MHz to 3.5 GHz, and more than -14.5 dB port isolation from 0.8 to 2.45 GHz. The slight discrepancy observed between the simulated and the measured s-
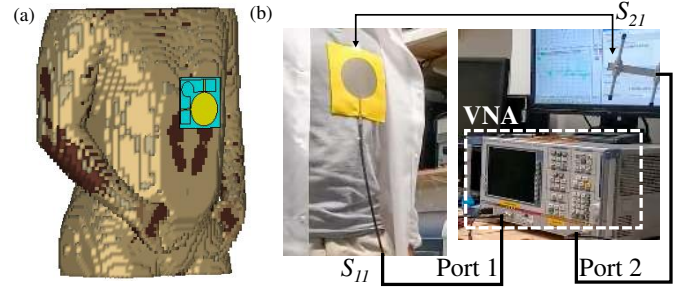

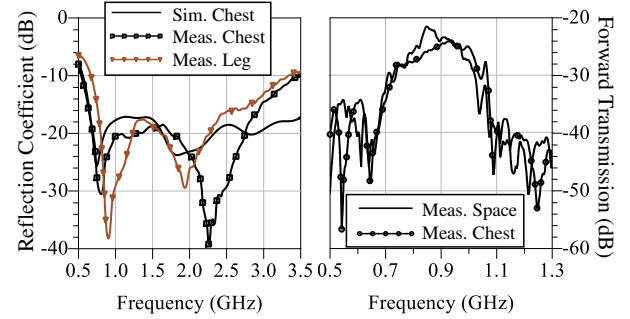Fig. 6. Antenna on-body simulation model (a), and measurement setup (b).

Fig. 7. S-parameters of the wearable antenna: (left) simulated and measured S_{11} on-body, (right) S_{21} between the textile antenna and a 10 dBi 900 MHz log antenna at 1 m.

parameters is due to the non-uniformity of the coax-microstrip interface at the SMA connector, due to the high-flexibility of the substrate.

As the antenna is designed to maintain broadband operation, it is not possible to shield the antenna using a solid ground plane or an unconnected reflector. Such conductive-backing would result in a narrow-band response similar to a microstrip patch antenna. In addition, it is desired to have wide angular coverage to be able to harvest arbitrarily-directed plane waves [14]. In human-proximity, it has been shown that the resonance of monopole antennas can shift by over 20% at 2.4 GHz [21]. Therefore, it is essential to measure the reflection coefficient of the antenna when operating on-body.

The antenna has been mounted on a user's chest with a non-uniform separation of $\approx$1 mm gap of clothing and air as shown in Fig. 6-b. A human model, AustinMan [42], was included in the antenna's 3D model in CST to simulate the gain (Fig. 6-a). Fig. 7-a compares the measured reflection coefficient of the antenna on-chest and on-leg with the simulation using the AustinMan. The measurement on-leg includes bending across a $\approx$7 cm radius. Both the simulation and measurement agree in showing a $S_{11} < -10$ dB from 0.8 to 3.5 GHz. The discrepancies below -15 dBm could be attributed to additional crumpling of the antenna prototype and additional mismatch at the SMA.

Certain placements on the body imply that the antenna may be bent over a sharper radius than that in Fig. 7, where the forward transmission was measured on-chest. It has previously been demonstrated that placing energy harvesting antennas on the extremities of the body (i.e. arm or leg) results in improved off-body link budget [15]. Fig. 8 shows the antenna's S_{11}
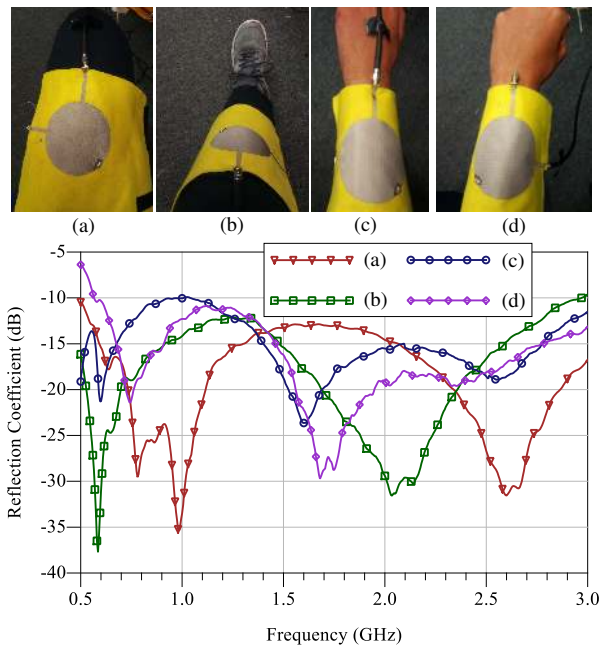
Fig. 8. Measured antenna's S_{11} during bending over various body parts: (a) 70 mm bending radius the y-axis on-thigh, (b) 55 mm bending radius on the y-axis on-leg, (c) 30 mm bending radius on the y-axis on-wrist, (d) 30 mm bending radius on the x-axis on-wrist

Fig. 9. Simulated SAR of the antenna on the Austinman phantom at 20 and 10 dBm, normalized to 1 gm.

while being bent over various body parts over radii between 70 and 30 mm. It can be seen that the antenna maintains its broad bandwidth over all body placements. The antenna was simulated on the Austinman model's arm with a 50 mm bending radius showing -2.21, 2.78 and 3.07 dB gain at 0.8, 1.5, 2.2 GHz, respectively, compared to -3.87, -0.28, and -0.68 dB, when placed flat on the model's chest. The higher on-arm gain agrees with the previously reported measurements showing improved antenna gain when placed on the arm compared to on-torso placements for both a monopole and a microstrip patch [15].

In addition to impedance matching, the degradation in an antenna's realized gain in proximity with the human body needs to be quantified. The forward transmission (S_{21}) between the textile antenna and a 10 dBi log-periodic antenna has been measured at 1 m separation, as shown in Fig. 6-b. The measured S_{21} is shown in Fig. 7-b. At 846 MHz, the maximum degradation in the gain is observed with the on-chest S_{21} (Fig. 6), and is 4.4 dB lower than that measured in space.

The measured gain, based on the free-space losses at 1 m and the 10 dB log antenna gain is -4.87 dB. This shows good agreement with the simulated antenna gain of -4 dB using the AustinMan model in Fig. 6-a. When the measurements were repeated to reduce the uncertainty due to multi-path reflections, the measured gain varied between -6.5 dB and -4 dB, on-body. Such variation could be attributed to subtle changes in the 1 mm separation between the antenna and the body.

An additional requirement in the design of wearable antennas is compliance with the Specific Absoprtion Rate (SAR) regulations. This is particularly relevant as the proposed antenna is unisolated from the body. Therefore, the power levels
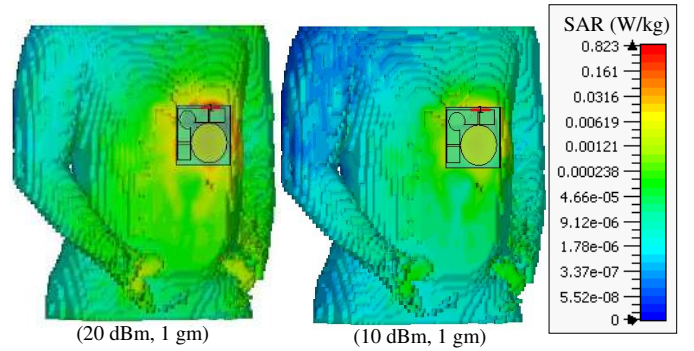
at which the antenna can be used safely are simulated in CST Microwave Studio to calculate the antenna's SAR. Fig. 9 shows the simulated SAR of the on-chest antenna; the peak SAR for a received/transmitted power of 20 and 10 dBm is 0.876 and 0.088 W/kg, respectively, when normalized to 1 gm of tissue mass. Both values are well below the 1.6 W/kg limit for mobile phones in the U.S.

Since the antenna will be used to receive and convert power as a rectenna, the 50Ω port connection is replaced with a connection to the rectifier. The rectifier requires a shunt current return path, before the diode, for the DC currents [43]. Such a return path could be achieved using a shunt inductor in the matching network. However, this requires an additional through-textile via which would complicate the fabrication process. To mitigate this, the current return path is built into the antenna. As the antenna is broadband, an additional ground-shorting textile wire could be connected between the monopole's disc and the bottom ground plane, without reducing the S_{11} bandwidth. The ground shorting thread added to the antenna is shown in the photograph in Fig. 4-a and b (GND-short). The s-parameters in Fig. 7 were measured after the GND-short thread was added which does not affect the impedance matching.

IV. TEXTILE MICROSTRIP RECTIFIER

A. Rectifier Design and Modeling

In order to harvest power efficiently, the impedance of the rectifier needs to be matched to the source (the antenna). Reported rectifier designs have focused on designing a rectifier first, computing or measuring its input impedance, then designing a 50Ω matching network or a complex conjugate antenna to match the rectifier's input impedance. While this approach achieves a good impedance match and high PCE, the design of the rectifier should not be input-impedance agnostic, as the PCE of a rectenna is not only dependent on the return loss (S_{11}) and the diode's parameters, but also on the source and load impedances.

The input impedance of a single series diode is typically very high, approaching open-circuit impedance at lower-frequencies. Nevertheless, the impedance values reported in RFEH studies and from diode manufacturer's measured s-parameters vary significantly between 1000Ω to 10Ω. This is
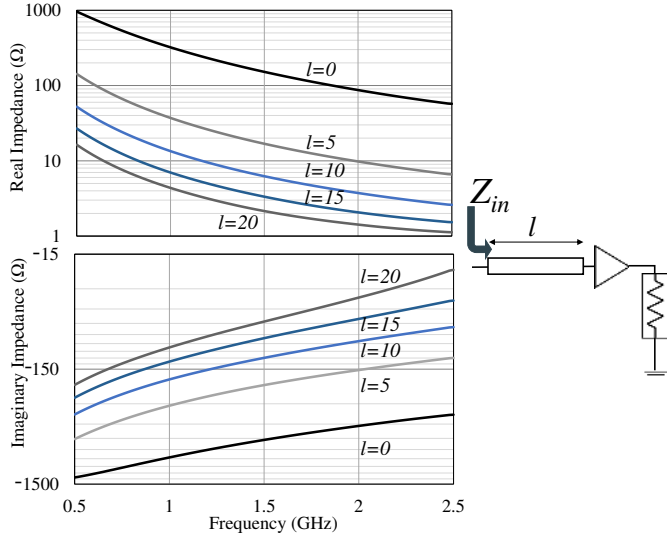
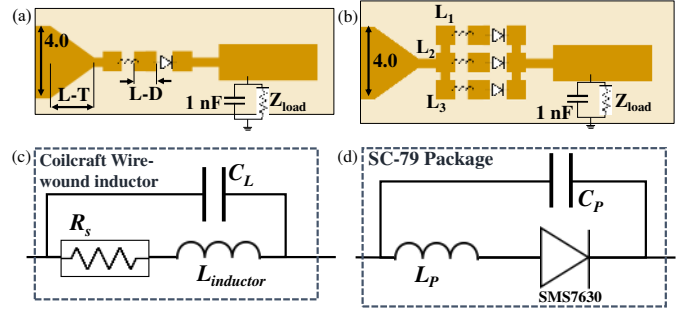Fig. 10. Single-series rectifier input impedance variation with the microstrip feed-length, l, in mm.

Fig. 11. Layout of the proposed microstrip rectifiers: (a) single-band, (b) multi-band, (c) equivalent circuit of a lumped matching inductor, (d) equivalent circuit of a packaged diode.

attributed to the quarter wave transformer effect introduced by the 2-port network, i.e. feed-line, any lumped components, or packaging parasitics between the input port and the diode's junction. This network can be represented as a line of length l, and impedance Z_l, varying the observed input impedance as in (1),

$$Z_{in} = Z_0 \frac{Z_l + jZ_0 tan(\beta l)}{Z_0 + jZ_L tan(\beta l)}, \tag{1}$$

making it more difficult to achieve a broadband impedance match.

For simplicity, considering a 50Ω air-dielectric microstrip feed-line of length l, for $0 < l < \lambda/4$ (typical for most commonly used lines below 3 GHz), any increase in l will result in a reduction of the observed input impedance, subsequently resulting in increased variation in the input impedance, due to the more variable range of frequencies to be matched in cellular RFEH. Fig. 10 shows the input impedance of a single-series rectifier, based on the SMS7630-079lf diode with different microstrip feed lengths, as seen by a 50Ω port.

It can be observed that although the real impedance approaches short circuit impedance as l approaches $\lambda/4$, the imaginary impedance sustains a higher capacitive component due to the diode's junction and packaging parasitic capacitance. While this can be factored in the matching process, a predominantly reactive source impedance will limit the maximum achievable PCE of the system [18]. Thus, operation in the diode's resistive region allows achieving higher PCE using the same diode. In addition, varying the length between the diode and the matching components can lower the observed input impedance. This makes matching a 50Ω antenna or port easier.

As this rectenna is optimized for maximizing PCE rather than voltage sensitivity, in the sub-100 μW range, the rectifier topology of choice is a single series rectifier. To add, the low voltage output of a single-series rectifier can be boosted using a high-efficiency low-power boost converter as in [4]. Further-

more, an additional advantage of a single-series rectifier is its high impedance ($\Re\{Z\}$) compared to a voltage doubler [44], enabling easier input matching over a wider bandwidth. The chosen diode is the Skyworks SMS7630-079lf, a low-barrier Schottky diode usable up to 9 GHz, due to its low series resistance and junction, resulting in a low forward voltage ($0.06 < V_f < 0.12$ mV for 0.1 mA [4]). Thus, it has been widely utilized in high-efficiency low-power rectennas [4], [14], [38]. As this work focuses on low-power RFEH, where the power levels expected rarely exceed −10 dBm [34], [38], [39], the relatively low breakdown voltage of the diode which will result in reduced PCE at higher power levels does not represent a practical issue.

B. High Impedance-Transformer Matching

From Fig. 10, it can be seen that a feedline of 5 mm length can transform the observed $\Re\{Z_{in}\}$ to 50Ω. Higher order distributed element networks were avoided due to the expected insertion losses in the lossy textile substrate [36]. Furthermore, while broadband matching has been reported using complex matching networks [35], [38], [39], [45], a triple-path rectifier is implemented to achieve the multi-band operation for harvesting power from different bands, without increasing the size or order of the matching network.

An ideal series inductor, of impedance $Z = j\omega L$, can match $\Im\{Z_{in}\}$, while the microstrip network can match the real high impedance of the rectifier (Fig. 10). In reality, a packaged lumped inductor carries associated capacitive and resistive parasitic components, as shown in Fig. 11-c. Therefore, accurate modeling of the inductor's parasitics, similar to the diode's parasitics in Fig. 11-d (usually given by the manufacturer) is required to obtain a close match between the simulation and analytical models and the measured results.

C. Single and Multi-Band Rectifiers

Two microstrip rectifiers with 50Ω input matching are designed for the felt substrate, to be etched as described in section II-A. The rectifiers are a 820 MHz (5G and LTE frequency in the U.K.) single-band single-path rectifier, and a multi-band triple-path rectifier matched at 940 MHz, 1.5 and 2.1 GHz. The layout of the proposed rectifiers is shown in Fig. 11, where the 50Ω microstrip feed is connected to the output of
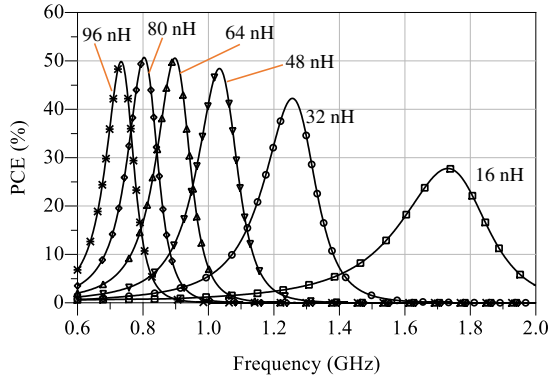
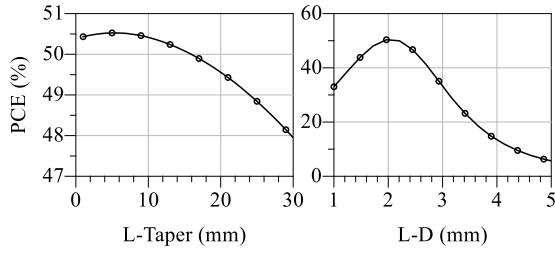Fig. 12. The rectifier's −20 dBm PCE as a function of frequency for different matching inductor values.

Fig. 13. The rectifier's −20 dBm PCE as a function of the microstrip taper length (L-T: left) and the length between the inductor and the diode (L-D: right).

the fully-textile antenna using the conductive fabric to flexible PCB transition shown in Fig. 3. The values of the matching inductors in Fig. 11 are L=82 nH for the single-band rectifier, and L_1=56 , L_2=20, L_3=11 nH for the multi-band rectifier. The choice of inductance, taper length (L-T) and separation between the inductor and diode (L-D) are discussed in the next section.

V. RECTIFIER SIMULATION AND MEASUREMENTS

A. Large-Signal Rectifiers' Performance

The rectifiers have been simulated using harmonic balance in Keysight ADS, based on the datasheet model for the diode's characteristics. The packaging parasitic inductance and capacitance have been obtained from the datasheet as well as the mismatched diode's S_{11} measurement, using a high-power VNA, based on the method described in [44]. The two designed rectifiers, the single and the triple-band have been simulated using closed-form microstrip-models for accurate modeling of the soldering pads, in the layout, and the feed point from the 50Ω source.

The initial values for L-T an L-D in Fig. 11-a are 2.5 and 0.5 mm, respectively. A parameter sweep of different inductances has been performed to maximize the PCE at −20 dBm as in Fig. 12. This process ensures a proper $\Im\{Z\}$ match is obtained. The next step is tuning the microstrip layout to maximize the $\Re\{Z\}$ match. Fig. 13 shows the PCE as a function of the microstrip taper and pad between the diode and the inductor. As previously shown in Fig. 10, a longer feed line (L-D) will result in a lower observed $\Re\{Z\}$. The
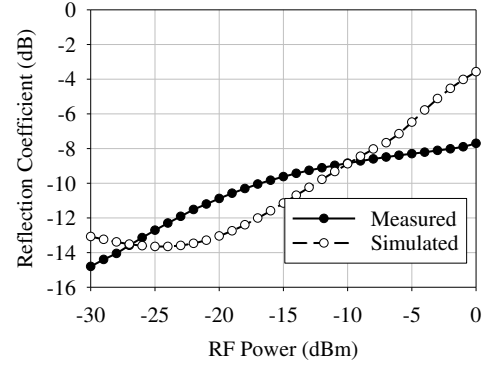

Fig. 14. Simulated and measured reflection coefficient (S_{11}) of the single band rectifier at different RF power levels from the CW VNA.
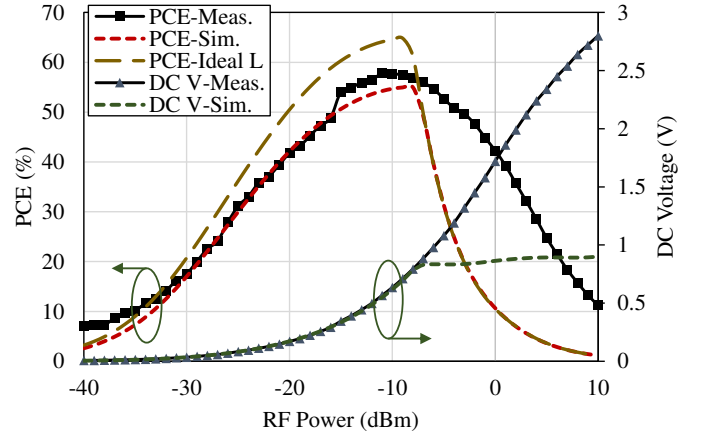

Fig. 15. Simulated (dashed) and measured (solid) PCE and DC voltage output of the single-band textile rectifier, at 820 MHz, with a 7 kΩ load resistor.

optimal values for L-T and L-D demonstrate that a compact rectifier will achieve the highest PCE. Such compactness gives the additional advantage of mitigating the insertion losses associated with the fabric substrate.

A Continuous Wave (CW) output from the VNA has been used to measure the large-signal reflection coefficient of the single-band rectifier and compare it with the simulated model, across a 7 kΩ. The matching inductors were simulated using both an ideal model with C_L=0.1 pF and the manufacturer s-parameters. An additional C_L component of 0.07 pF was added post-measurement to the s-parameters model. Fig. 14 shows the reflection coefficient of the rectifier, demonstrating an improved impedance-match in the low power region, corresponding to the design range of this work. Given the optimized impedance match for −20 dBm, it is expected that the proposed rectifier achieves higher PCE compared to reported rectifiers utilizing a similar diode, with a generic matching network. Fig. 15 shows the measured PCE of the single-band rectifier demonstrating high PCE at 10 μW power levels. Based on the simulation using an ideal inductor in Fig. 15, the maximum achievable PCE at −20 dBm is 50%.

To demonstrate the reliability of the proposed rectifier, the DC measurements were repeated over multiple bending cycles. Repetitive bending of textile-based electronics is widely used as a reliability test [31]. Five bending cycles of the rectifier
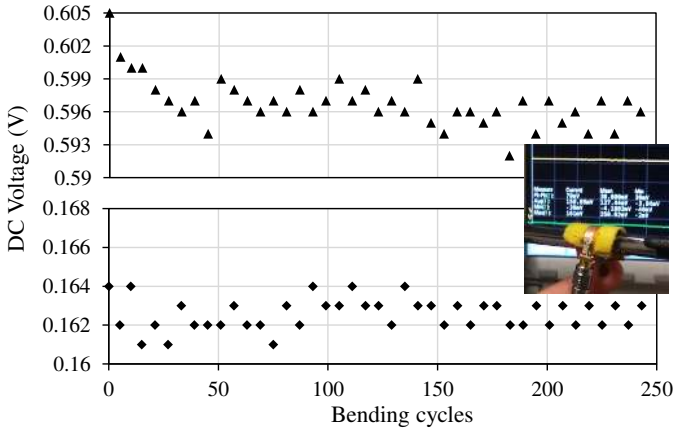
Fig. 16. Measured DC output at -10 (top) and -20 dBm (bottom) for repetitive bending cycles; inset shows photograph of the bent rectifier.
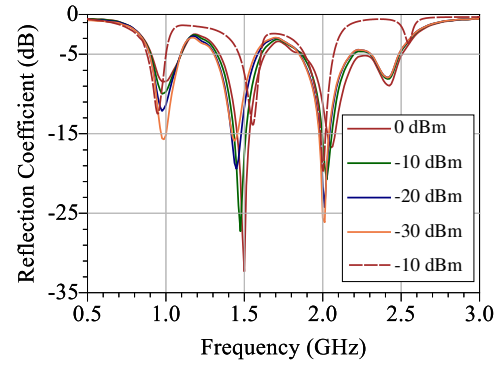

Fig. 17. Measured (solid) and simulated (dashed) reflection coefficient of the multi-band rectifier.
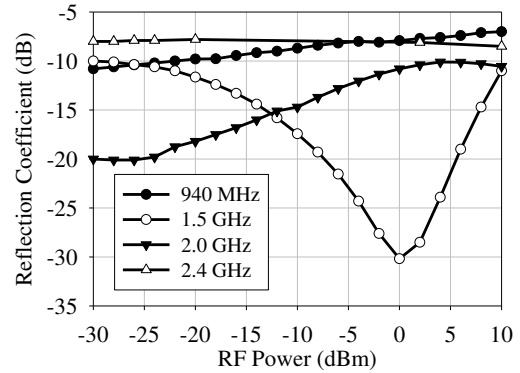

Fig. 18. Measured large-signal reflection coefficient of the multi-band rectifier with variable input power levels, at the frequencies where a resonance was observed.

prototype in Fig. 2-e were performed before the DC output was measured at -20 and -10 dBm. Fig. 16 shows the measured DC voltage for 250 bending cycles. Each bending cycle was performed at a sharp bending radius of $<$5 mm, the DC voltage was measured during and after bending and no noticeable difference was observed. The maximum variation for both -20 and -10 dBm was less than 3%, and did not resemble a permanent or cumulative degradation. Such a reliability test demonstrates the rectifier's suitability for the harshest wearable applications, and is in line with the reliability tests of electronic textiles in [31].

To investigate the losses associated with the textile-based interconnects, the single-band rectifier has been prototyped on a standard FR4 PCB. The DC voltage of the textile rectifier at -20 dBm was only 4.6% lower than that of a its rigid counterpart. This translates to less around 1% PCE-improvement when migrating to a rigid substrate, concluding that compact lumped matching enables mitigation of the insertion losses associated with textile transmission lines and low-cost substrates. As FR4 is a lossy substrate, the purpose of this is to demonstrate that interconnects on textile do not affect the performance. Moreover, the rectifier's has been simulated for a tanδ=0 substrate and the -20 dBm PCE was 44.5% as opposed to the 41.8% measured PCE of the proposed textile-based rectifier.

The multi-band rectifier (Fig. 11-b) has been connected to a VNA to measure its bandwidth and evaluate its performance, Fig. 17 shows the measured reflection coefficient of the rectifier at different input power levels. As with the single-band rectifier, it is observed that the reflection coefficient changes with the available RF power, due to the variation in the diode's input impedance. For example, at 960 MHz (GSM RFEH band) it is observed that the rectifier is optimized for -20 dBm and below. On the other hand, the inductive matching at 1.5 GHz improves at higher power levels (minimum reflection is achieved at 0 dBm). This is due to the diode's lower impedance at higher frequencies and the inductors approaching their self-resonant frequencies where the inductance is higher than the datasheet values. The low self-resonant frequency is due to the lower frequency matching inductor. The 56 nH 0603 Coilcraft

inductor used for matching at 960 MHz self resonates at 1.9 GHz, which may result in additional interference with the high frequency rectifier path. Fig. 18 shows the measured large-signal reflection coefficient of the rectifier at the four bands where a drop in the S_{11} is observed.

The multi-band rectifier, despite being well-matched at three frequency bands (cellular and ISM-bands), suffers from reduced PCE at both sub-100 μW levels (the design range of the single-band rectifier) and at their peak PCE, as a result of the additional multi-path reflection. To explain, the frequency-selective multi-path rectifier results in additional current flow of the RF signal in the microstrip network as well as the lumped components, due to the impedance mismatch of every other branch happening at the diode's plane rather than the microstrip cross-junction. This is attributed to the microstrip lines' short length compared to the wavelength, resulting in the signal traveling towards the diodes before being reflected and finally accepted by their respective branch based on the frequency. In addition, unintended resonance observed at 2.4 GHz is due to the mutual-inductance between the three paths and hence does not contribute to the DC output. While it is possible to use open stubs to suppress harmonics at the output, open stubs are not included to keep the rectifier compact and minimize the circuitry covering the textile. Lack of harmonic termination is the reason the 2 GHz PCE degrades to about 50% of that at 0.96 and 1.5 GHz. Fig. 19 shows the PCE of
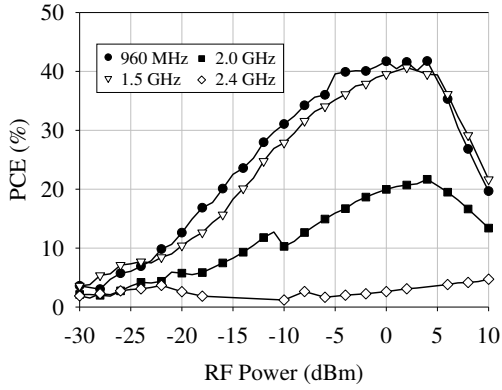
Fig. 19. Measured PCE of the multi-band rectifier, at the different frequencies where a resonance is observed, with a 4.7 kΩ load.
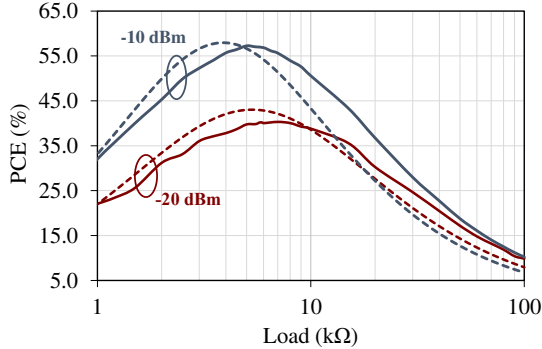

Fig. 20. Measured (solid) and simulated (dashed) PCE of the proposed single-band rectifier.

Fig. 21. Measured (solid) and simulated (dashed) PCE of the multi-band rectifier at (a) 960 MHz and (b) 1.5 GHz.

the rectifier at variable RF power levels.

From Fig. 19, it is observed that the PCE diminishes at higher frequencies, which is attributed to the mutual coupling between the tightly-positioned matching inductors. To illustrate, the higher-value inductor L_1 has a self-resonant frequency below 2 GHz, resulting in a smaller portion of the incident high-frequency signal being accepted by the diodes, hence reducing the PCE. This highlights the limitation of multi-band inductive matching using non-ideal components.

B. Resistive DC Load Sweep

As the rectifier's performance is expected to vary significantly based on the load impedance, the performance of the proposed rectifiers have been investigated for various resistive loads, as well as a capacitive load acting as an energy storage unit directly connected to the rectenna, eliminating the DC power management stage. A DC resistive load sweep has been carried out experimentally and in simulation to find the rectenna's optimal load impedance for both the single-band and multi-band rectifier. Fig. 20 and 21 show the PCE at variable load impedance at −20 and −10 dBm input power.

From Fig. 20, the proposed rectifier achieves a best-in-class PCE of 41.8% at −20 dBm with a 7 kΩ load, in good agreement with the simulated maximum PCE of 43% at the same frequency. The load impedance of the rectifier is in line with other rectennas such as [4] and [39] and allows a
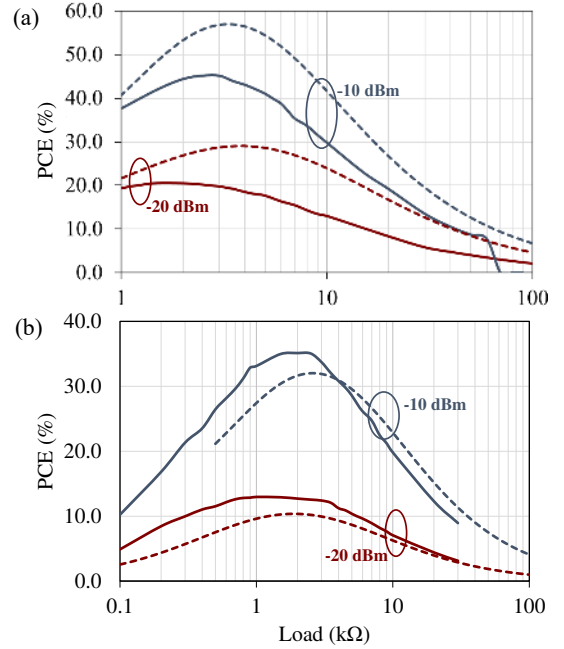
balance between the DC voltage output and a high PCE This is achieved due to the optimized impedance matching for low RF power levels and the high-impedance end-to-end environment described in section IV-B. Additionally, more than 10% of the maximum PCE is maintained from 2.5 to 14 kΩ and 3.0 to 13.3 kΩ at −10 and −20 dBm respectively. Finally, the validity of the inductor's equivalent model proposed in Fig. 11-c is validated across varying Z_{load}.

The multi-band rectifier's model exhibits discrepancies with the measured results especially at 960 MHz, due to the resonance shift previously observed in the S_{11} (Fig. 18). The fabricated rectifier prototype, despite achieving more than 20% and 45% PCE at 960 MHz which is in-line with reported values using the same rectenna, fails to achieve the simulated PCE approaching 60% at −10 dBm. This can be attributed to the tight spacing (<1 mm clearance) of the "lumped" inductors, resulting in a considerable mutual-inductance component as well as coupling between the rectifier's branches causing additional stray currents dissipating in the inductors' parasitics and the fabric substrate. The manufacturer's measured s-parameters of the coil clearly exclude the effects of other components in proximity as well as the effect of external interconnects resulting in variable C_L.

C. Rectifier Capacitive Load Analysis

Energy storage is essential in energy harvesting and intermittently-powered systems to enable cold-start of a battery-free load. Therefore, it is essential to characterize the performance of RF rectifiers directly with a capacitive load. While recent studies have investigated the charging time of a capacitor using a low-power rectenna [16], using a power-management circuit masks the capacitor's current draw and
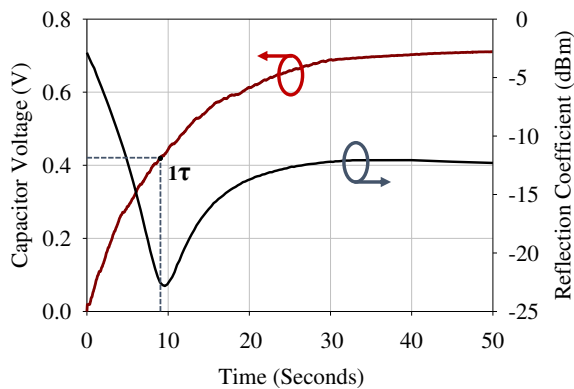
Fig. 22. 1.32 mF C_{Store} charging time and the measured reflection coefficient variation with the energy stored in the capacitor over time from -10 dBm.
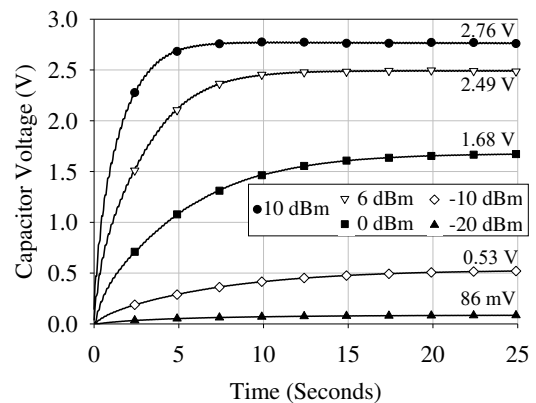

Fig. 23. Measured voltage across the 1.32 mF capacitor during charging using the 970 MHz RF power, and the peak voltage reached at different power levels.

does not give any insight on the impact of the charging curve on a rectifier's S_{11}.

Motivated by keeping the component count low in the system to improve its flexibility and reliability, a discrete power management interface is avoided. Furthermore, multiple state-of-the-art low-voltage transceivers and micro-controllers have been reported with turn-on voltages as low as 250 mV [46]. Thus, the output voltage of the rectenna could be directly stored without stepping-up using a DC-DC boost converter.

A storage capacitor, C_{store}, has been connected directly to the output of the microstrip rectifier replacing Z_{Load}. C_{store} is implemented using electrolytic capacitors of 1.32 mF capacitance, measured using an impedance analyzer at various frequencies from 20 Hz to 1 kHz. The performance of the single-band rectifier, with C_{Store} replacing the dummy resistive load, has been experimentally measured. The charge level in the capacitor affects its ability to be charged from a voltage source. Thus, the equivalent input impedance of the capacitor will vary during the charging cycle changing the rectifiers S_{11}. Considering the difficulty in modeling the internal DC and RF parasitics of the electrolytic capacitors, simulation of the capacitive load was not performed. A VNA has been used in CW mode as a power source to excite the single-band rectifier, while measuring the reflection at the input. As the large-signal input impedance of the capacitor is not known, it is crucial to measure the input reflection coefficient to ensure the capacitive load does not degrade the rectenna's impedance match. The DC voltage across the capacitor has been measured using an oscilloscope during the charging time of the capacitor, until a steady state voltage is reached. Fig. 22 shows the charging time of the capacitor and the variation in the measured S_{11} with the amount of charge in the capacitor at -10 dBm.

From the moment the VNA is turned-on (time=0), it is observed that the reflection coefficient of the diode changes significantly based on the amount of charge stored in the capacitor, implying an input impedance change. This can be explained by the charging curve of a capacitor, where initially the current (2) is significantly higher than the voltage. The current flowing into the capacitor given by

$$I_C = \frac{V}{R} e^{\frac{-t}{RC}} \qquad (2)$$

will determine the load impedance and subsequently the rectifier's S_{11}.

The optimal impedance match ($S_{11}=-23$ dB) is achieved at time=τ, from τ=RC and the measured capacitance, the DC resistance of the circuit at that instance can be worked out to be 6212Ω, closely approaching the optimal load impedance of the single-band rectifier shown in Fig. 20. The low reflection observed after the steady-state voltage is reached is due to the high leakage of electrolytic capacitors, resulting in a continuous current draw from the rectenna to maintain the energy stored.

The energy stored in the capacitor can be used to calculate the average PCE of the rectenna with capacitive loading (3), where the average charging power from the rectenna during the first RC time constant, τ, is compared to the available RF power.

$$PCE_{average} = \frac{C_{Store}V^2}{2} \times \frac{1}{\tau} \times \frac{1}{P_{RF}} \qquad (3)$$

The calculated efficiency of the capacitor-loaded rectifier at -10 dBm is 15.3% compared to 54% of the resistive-loaded rectifier at the same power level. The significantly lower PCE is attributed to the variation in the capacitor's impedance affecting both the RF impedance matching at the rectenna's input (Fig. 22) and the DC power transfer between the rectenna and the DC load.

An input power sweep has been carried out from -20 to 10 dBm to investigate the variation in $PCE_{Average}$ for a capacitive load. The charging curves of the load capacitor can bee seen in Fig. 23 for different power levels. The power sweep oscilloscope traces were used to extract the RC time constant at different power levels to calculate the average PCE using (3). Fig. 24 shows the measured peak capacitor voltage and the voltage at the first τ, in addition to the average PCE (3).

The diminished PCE of the rectifier with the C_{store} as a load is mainly observed at lower power levels due to the wide variation in the input impedance demonstrated through the variation of the S_{11} over time in Fig. 22. This prohibits a
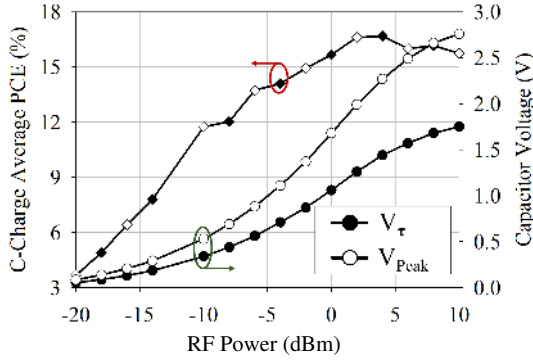
Fig. 24. The measured average PCE of the capacitive-load rectifier and the capacitor voltage at the first time constant and the peak voltage.

VI. RECTENNA WIRELESS TESTING AND EVALUATION

In order to demonstrate the performance of the whole textile rectenna (antenna and rectifier), the dual-LP broadband monopole is integrated with the proposed rectifier using the textile transition from Fig. 3. This section presents the wireless testing and evaluation of the integrated textile rectenna shown in Fig. 2-a. The tests carried out in this section demonstrate:

1) High PCE of the rectenna in space and on-body for sub-μW/cm^2 power densities.
2) Dual-polarization harvesting capabilities.
3) Omnidirectional power reception capabilities.

A standard 10 dBi LP log-periodic antenna has been used to illuminate the antenna with RF power over a fixed distance d, while varying the power available from the VNA configured to act as a CW generator. Given the VNA's maximum leveled output of 15 dBm, the distance d has been set to 1.2 m to be able to deliver power densities up to 1.75 μW/cm^2 to the rectenna. A distance of 1.2 m represents $3.3\times\lambda$ at 820 MHz, ensuring the antennas are in their farfields. The setup is consistent with the test setups in [16] and [1], where the transmitter-rectenna separation was 1.2 and 1 m, respectively. Fig. 25 shows the test setup of the textile rectenna.

The power density S at the antenna has been calculated using (4)-(5) from the incident electric field E given by

$$S = \frac{E^2}{120\pi}; \tag{4}$$

$$E = \frac{\sqrt{30P_T G_t}}{d}, \tag{5}$$

where P_T and G_T are the transmitter's power and gain, respectively.

The power received by the rectenna, a function of the antenna's effective area A_{eff} (7) and the RF power density S, has been used to calculate the PCE for an incident plane wave PCE_{plane} (6). The PCE from a plane wave has been calculated using A_{eff}, using the measured gain G_R in space and on-body. PCE_{plane} is given by
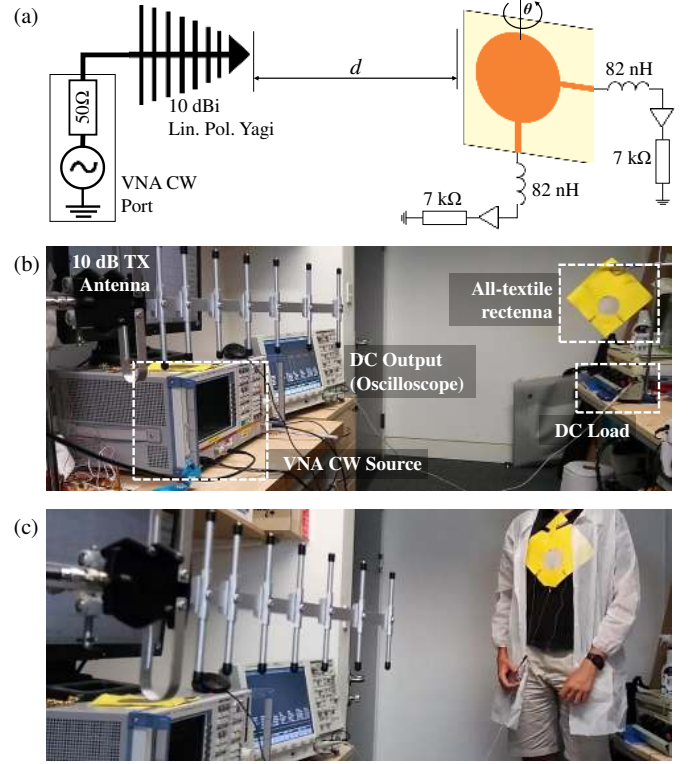

Fig. 25. The wireless test setup of the textile rectenna: (a) schematic of the wireless test setup, (b) photograph of the rectenna testing in space, (c) photograph of the rectenna testing when mounted on-body.

$$PCE_{plane} = \frac{P_{DC}}{SA_{eff}}, \tag{6}$$

$$A_{eff} = G_R \frac{\lambda^2}{4\pi}. \tag{7}$$

When measuring the PCE for the misaligned polarization case, A_{eff} is halved due to the -3 dB PML. PML reduces the RF power received by each port by 50% which is then overcome by combining the power output of both ports [41]. When performing the on-body measurements, the -6.5 dB worst-case measured gain was used in the calculations.

A power sweep has been carried out to measure the received DC power and PCE at variable incident power densities. The CW input has been swept from -6 to 15 dBm. The measurements were performed with the rectenna positioned in free space and mounted on-body as in Fig. 25-b and 25-c. The antenna's position on the torso reflects the position with the lowest antenna efficiency [15]. Thus, it is the most conservative estimate of the antenna's wearable performance.

Fig. 26 shows the measured PCE and DC output of the rectenna at 820 MHz for a 7 kΩ load. It is observed that the antenna achieves a PCE surpassing 50% and 45% from $S < 1$ μW/cm^2 in space and on-body, respectively. Compared to other all-textile rectennas [1], [5], [6], this work presents the only rectenna capable of efficient power generation for power densities below 1 μW/cm^2 despite lack of shielding, having a low profile, and the smallest electrical area.

The next step in evaluating the rectenna is to validate the performance for polarization misalignments. The transmitting
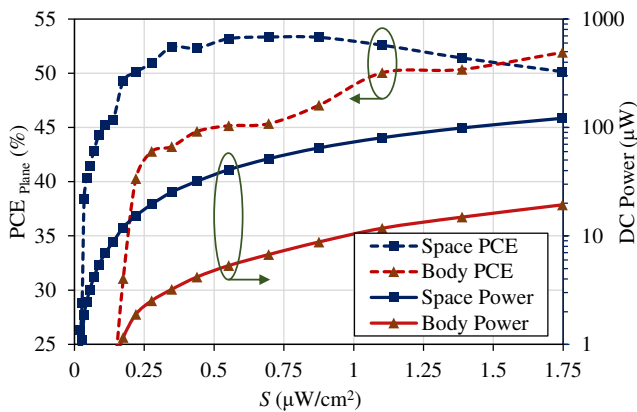
Fig. 26. Measured DC output and PCE of the textile rectenna on-body and in space from varying plane-wave excitations.
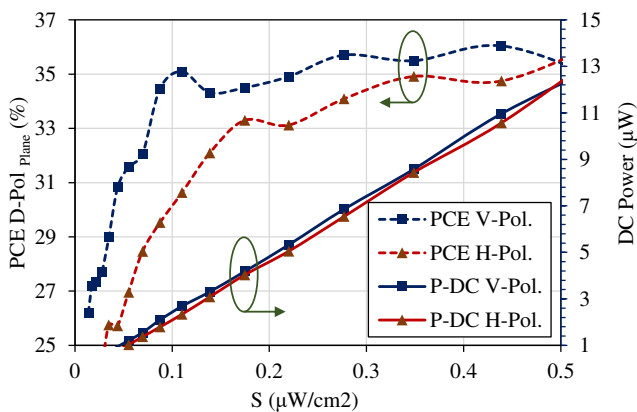

Fig. 27. Measured DC output and PCE of the textile rectenna across both ports for variable incident plane waves with 45° polarization angle.

antenna has been rotated to have a 45° angle. To verify that the incident wave is 50% misaligned with both ports of the rectenna a connectorized textile antenna was used to measure the forward transmission at both ports. The measured S_{21} at both ports was verified to be 3 dB lower than that when the polarization is fully-aligned. S has been swept while measuring the DC output of both ports.

Fig. 27 shows the measured PCE and DC output. It can be observed that, for the misaligned polarization case, the PCE is approximately 25% lower than a single-port output when the polarization is aligned. This is attributed to the mutual coupling between the ports as well as additional path losses linked to the positioning of the transmitter. The variation in the power output between the V-pol. and H-pol. could be attributed to slight variation in the polarization angle due to the transmitting antenna's position and indoor multi-path effects.

To demonstrate the omnidirectional harvesting properties of the antenna, the integrated rectenna is rotated around the axis shown in Fig. 25. The antenna is positioned at d=1.6 m and the VNA's CW output is set to 14 dBm, this results in a power density of 0.78 μW/cm^2. Fig. 28 shows the measured DC power output of the rectenna as well as the antenna's simulated gain at 820 MHz. It has previously been demonstrated that a rectenna's DC voltage patterns can vary significantly from the
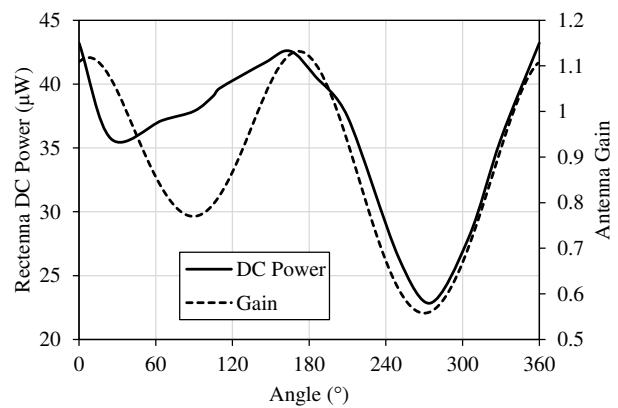

Fig. 28. Measured DC output of the rectenna for variable alignment angles with the directional transmitter and the antenna's gain.

antenna's RF radiation patterns due to the rectifier's size and layout [47]. In addition, planar and non-planar positioning of rectifiers was found to alter the received DC power [16].

In Fig. 28, very close agreement between the simulated gain and the DC power is observed from 180° to 360°. From 0° to 180°, the DC power output is about 50% higher than expected from the simulated gain, this could be attributed to the indoor test setup resulting in varying multi-path effects. From Fig. 28, it can be concluded that the proposed rectenna maintains omnidirectional power harvesting capabilities with the half-power beamwidth covering the entire 360° angular span.

Table I compares the proposed rectenna with state-of-the-art wearable rectennas with textile antennas [1], [3]–[6]. Two non-textile rigid rectennas are included in the table for bench-marking. [16] is a low-profile rectenna designed for ultra-low power densities, operating at a very close frequency to this work. [14] is a wide angular coverage 2.4 GHz rectenna based on a complex 3D structure with multiple patch arrays and a beamforming network.

It is clear that the proposed rectenna, despite being fully-implemented on textiles and utilizing an ultra-compact lumped matching network, achieves the highest reported PCE at −20 dBm, and subsequently for S<1 μW/cm^2. The PCE$_{\text{Plane}}$ presents over 5× improvement compared to reported un-isolated wearable rectennas such as [6]. The proposed rectenna also occupies the smallest electrical size compared to other textile rectenna due to its monopole antenna as opposed to patch antennas. As in Fig. 26, the lack of shielding did not prevent the rectenna from yielding over 10 μW from S=1 μW/cm^2. This shows that unisolated antennas can indeed be used for wearable energy harvesting. Compared to the complex 3D quasi-omnidirectional rectenna in [14], the proposed low-profile low-cost rectenna still maintains 360 3 dB beam-width (Fig. 28) based on the omnidirectional antenna. The higher DC output, from the same S, compared to [14] is due to the high PCE of the proposed rectifier.

VII. CONCLUSION

Realizing a high-efficiency complete wireless power harvesting system based using textile-based RF components has been a significant research challenge. This paper presented a

TABLE I
COMPARISON OF THE PROPOSED TEXTILE RECTENNA WITH REPORTED WEARABLE AND LOW-POWER RECTENNAS.

Study	Antenna Substrate	Rectifier Substrate	Frequency (GHz)	Diode	PCE at −20 dBm (%)	Loads investigated	PCE at S=0.5 μW/cm² (%)	DC P at S=0.5 μW/cm² (μW)	Half-power beamwidth	Electrical size (λ_0^3)
This work	Felt (all fabric)	Felt (polyimide on fabric)	0.82	SMS7630-079lf	41.8	Resistive/capacitive sweep	53	35	360°	0.329 × 0.329 × 0.0027
Monti TAP'13 [1]	Pile+Jeans (all fabric)	Jeans (all fabric)	0.876	HSMS-285X	NR	Resistive sweep	NR, 45 from 3	NR, 360 from S=2.5	80°*	0.702 × 0.556 × 0.0088
Adami TMTT'18[4]	Felt (all fabric)	Duroid 5880	2.45	SMS7630-079lf	33.6	Resistive sweep	NR	NR	60°*	0.74 × 0.39 × 0.028
Vital TAP'19 [5]	Felt (all fabric)	Felt (all fabric)	2.4	SMS7630-079lf	18	Single resistor	NR	NR	NR, ≈65°**	0.625 × 0.6 × 0.013†
Estrada TMTT'20 [6]	Cotton (all fabric)	Cotton (all fabric)	2-5	SMS7630-079lf	NR	Resistive sweep	<5%§	9 from S=4	omni-directional	NR, >1 × 1 × 0.0006‡
Okba TMTT'19 [16]	FR4	Durroid	0.85	HSMS2850	28*	Resistive sweep	31*%	20	80°×2	0.32 × 0.17 × 0.0045
Vandelle TAP'19 [14]	RO4003	RO4003	2.4	SMS7630-079lf	NR	Single resistor	40	18	344°	2.32 × (1.04 × 1.04 × π)

*Estimated from the graphs; ** typical patch beamwidth; †antenna only; ‡ estimated from the photographs; § PCE calculated using physical area, not A_{eff}

textile-based wearable rectenna achieving the highest reported PCE for sub-1 μW/cm² harvesting, surpassing both its textile and rigid counterparts. The proposed rectenna achieves a best-in-class PCE of 41.8% at 820 MHz from −20 dBm due to careful design of the rectifier and optimized matching for sub-100 μW power levels. The multi-band rectifier is studied under a variety of resistive and capacitive loads and is demonstrated charging an electrolytic 1.32 mF capacitor to 1-V in under 0.41 seconds from 10 dBm of power, along with investigation of its input impedance variation as part of the charging curve. The integrated rectenna is demonstrated with more than 35% PCE from an arbitrarily-polarized power density of 0.23 μW/cm², demonstrating its capability to harvest low RF power densities, while maintaining a 360° half-power beamwidth. .

Several novel contributions have been presented in this work. First of all, the use of an unshielded all-textile monopole to realize a high-efficiency wearable harvester with state-of-the-art PCE has not been presented in literature. In addition, the textile-based inductive-matched rectifier demonstrates that lumped components can enable high-efficiency rectennas on lossy substrates. Moreover, time-variant analysis of a rectifier using s-parameters while charging a capacitor is a new technique for evaluating RF harvesters. Finally, we have demonstrated the scalability of the proposed rectenna for multi-band operation, dual-polarization, and omnidirectional harvesting.

REFERENCES

[1] G. Monti, L. Corchia, and L. Tarricone, "UHF Wearable Rectenna on Textile Materials," *IEEE Trans. Antennas. Propag.*, vol. 61, 7, pp. 3869 – 3873, 2013.

[2] L. Corchia, G. Monti, and L. Tarricone, "Wearable Antennas: Non-textile Versus Fully Textile Solutions," *IEEE antennas propag. mag.*, vol. 61, 2, pp. 71 – 83, 2019.

[3] K. W. Lui, O. H. Murphy, and C. Toumazou, "A Wearable Wideband Circularly Polarized Textile Antenna for Effective Power Transmission on a Wirelessly-Powered Sensor Platform," *IEEE Trans. Antennas Propag.*, vol. 61 no. 7, pp. 3873 – 3876, 2013.

[4] S.-E. Adami *et al.*, "A Flexible 2.45-GHz Power Harvesting Wristband With Net System Output From -24.3 dBm of RF Power," *IEEE Trans. Microw. Theory Techn.*, vol. 66, 1, pp. 380–395, 2018.

[5] D. Vital, S. Bhardwaj, and J. L. Volakis, "Textile Based Large Area RF-Power Harvesting System for Wearable Applications," *IEEE Trans. Antennas Propag.*, vol. Early Access, 2019.

[6] J. A. Estrada *et al.*, "An RF-Harvesting Tightly-Coupled Rectenna Array Tee-Shirt with Greater than Octave Bandwidth," *IEEE Trans. Microw. Theory Techniq.*, vol. Early Access, pp. 1 – 1, 2020.

[7] T. C. Baum *et al.*, "Embroidered active microwave composite preimpregnated electronicspregtronics," *IEEE Trans. Microw. Theory Techniq.*, vol. 64, 10, pp. 3175 – 3186, 2016.

[8] X. Lin *et al.*, "Ultra-Wideband Textile Antenna for Wearable Microwave Medical Imaging Applications," *IEEE Trans. Antennas Propag.*, vol. 68 no. 6, pp. 4238 – 4249, 2020.

[9] A. Alemaryeen and S. Noghanian, "On-Body Low-Profile Textile Antenna With Artificial Magnetic Conductor," *IEEE Trans. Antennas Propag.*, vol. 67 no. 6, pp. 3649 – 3656, 2019.

[10] X. Tian *et al.*, "Conformal Propagation and Near-Omnidirectional Radiation with Surface Plasmonic Clothing," *IEEE Trans. Antennas Propag.*, vol. Early Access, 2020.

[11] C. X. Mao *et al.*, "Low-Profile Strip-Loaded Textile Antenna with Enhanced Bandwidth and Isolation for Full-Duplex Wearable Applications," *IEEE Trans. Antennas Propag.*, vol. Early Access, 2020.

[12] C.-X. Mao *et al.*, "Dual-Polarized Embroidered Textile Armband Antenna Array With Omnidirectional Radiation for On-/Off-Body Wearable Applications," *IEEE Trans. Antennas Propag.*, vol. 68 no. 4, pp. 2575 – 2584, 2020.

[13] M. Wagih, A. S. Weddell, and S. Beeby, "Rectennas for RF Energy Harvesting and Wireless Power Transfer: a Review of Antenna Design," *IEEE antennas propag. mag.*, vol. Accepted: In Press, 2019.

[14] E. Vandelle *et al.*, "Harvesting Ambient RF Energy Efficiently With Optimal Angular Coverage," *IEEE Trans. Antennas Propag.*, vol. 67, 3, pp. 1862 – 1873, 2019.

[15] M. Wagih *et al.*, "Real-World Performance of Sub-1 GHz and 2.4 GHz Textile Antennas for RF-Powered Body Area Networks," *IEEE Access*, vol. Early Access, 2020.

[16] A. Okba, A. Takacs, and H. Aubert, "Compact rectennas for ultra-low-

power wireless transmission applications," *IEEE Trans. Microw. Theory Techn.*, vol. 67, 5, pp. 1697 – 1707, 2019.

[17] C. R. Valenta and G. D. Durgin, "Harvesting Wireless Power: Survey of Energy-Harvester Conversion Efficiency in Far-Field, Wireless Power Transfer Systems," *IEEE Microw. Mag.*, vol. 15, 4, pp. 108–120, 2014.

[18] Y.-S. Chen and C.-W. Chiu, "Maximum Achievable Power Conversion Efficiency Obtained Through an Optimized Rectenna Structure for RF Energy Harvesting," *IEEE Trans. Antennas Propag.*, vol. 65, 5, pp. 2305 – 2317, 2017.

[19] H. J. Visser, S. Keyrouz, and A. B. Smolders, "Optimized Rectenna Design," *Wireless Power Transfer*, vol. 2, 1, pp. 44 – 50, 2017.

[20] X. Lin, B.-C. Seet, and F. Joseph, "Fine-pitch surface component mounting on screen-printed fabric circuits," *Electron. Lett.*, vol. 52 no. 12, pp. 1032 – 1034, 2016.

[21] M. Wagih, Y. Wei, and S. Beeby, "Flexible 2.4 GHz Sensor Node for Body Area Networks with a Compact High-Gain Planar Antenna," *IEEE Antennas Wireless Propag. Lett.*, vol. 17, 12, pp. 49 – 53, 2018.

[22] Y. H. Jung *et al.*, "A Compact Parylene-Coated WLAN Flexible Antenna for Implantable Electronics," *IEEE Antennas Wireless Propag. Lett.*, vol. 17, 12, 2018.

[23] P. Nepa and H. Rogier, "Wearable Antennas for Off-Body Radio Links at VHF and UHF Bands: Challenges, the state of the art, and future trends below 1 GHz," *IEEE antennas propag. mag.*, vol. 57 no. 5, pp. 30 – 52, 2015.

[24] H. Sun *et al.*, "Design of a High-Efficiency 2.45-GHz Rectenna for Low-Input-Power Energy Harvesting," *IEEE Antennas Wireless Propag. Lett.*, vol. 11, pp. 929–932, 2012.

[25] A. R. Guraliuc *et al.*, "Effect of textile on the propagation along the body at 60 ghz," *IEEE Trans. Antennas Propag.*, vol. 62, 3, pp. 1489 – 1494, 2014.

[26] M.-Q. Lee and S. Nam, "An accurate broadband measurement of substrate dielectric constant," *IEEE Microwave and Guided Wave Letters*, vol. 6, 4, pp. 168 – 170, 1996.

[27] F. Declercq, H. Rogier, and C. Hertleer, "Permittivity and loss tangent characterization for garment antennas based on a new matrix-pencil two-line method," *IEEE Trans. Antennas Propag.*, vol. 56, 8, pp. 2548 – 2554, 2008.

[28] K. Yang *et al.*, "Waterproof and durable screen printed silver conductive tracks on textiles," *Textile Research Journal*, vol. 83, pp. 2023 – 2031, 2013.

[29] W. G. Whittow *et al.*, "Inkjet-Printed Microstrip Patch Antennas Realized on Textile for Wearable Applications," *IEEE Antennas Wireless Propag. Lett.*, vol. 13, pp. 71–74, 2014.

[30] M. Wagih *et al.*, "Broadband Millimetre-Wave Flexible Textile-based Rectenna for Wearable Energy Harvesting ," *IEEE Trans. Microw Theory Techn*, In Review.

[31] A. Komolafe *et al.*, "Integrating flexible filament circuits for etextile applications," *Advanced Materials Technologies*, vol. 4, no. 7, 2019.

[32] M. Wagih *et al.*, "Reliable UHF Long-Range Textile-Integrated RFID Tag Based on a Compact Flexible Antenna Filament," *Sensors*, vol. 20 (12), p. 3435, 2020.

[33] R. Seager *et al.*, "Flexible radio frequency connectors for textile electronics," *Electronics Letters*, vol. 49, no. 22, pp. 1371 – 1373, 2013.

[34] M. Pinuela, P. D. Mitcheson, and S. Lucyszyn, "Ambient RF Energy Harvesting in Urban and Semi-Urban Environments," *IEEE Trans. Microw. Theory Techn.*, vol. 61, 7, pp. 2715 – 2726, 2013.

[35] H. Sun *et al.*, "A Dual-Band Rectenna Using Broadband Yagi Antenna Array for Ambient RF Power Harvesting," *IEEE Antennas Wireless Propag. Lett.*, vol. 12, pp. 918 – 921, 2013.

[36] V. Palazzi *et al.*, "A Novel Ultra-Lightweight Multiband Rectenna on Paper for RF Energy Harvesting in the Next Generation LTE Bands," *IEEE Trans. Microw. Theory Techn.*, vol. 66, 1, pp. 366 –379, 2018.

[37] S. Shen, C.-Y. Chiu, and R. D. Murch, "Multiport Pixel Rectenna for Ambient RF Energy Harvesting," *IEEE Trans. Antennas Propag.*, vol. 66, 2, pp. 644 –656, 2018.

[38] C. Song *et al.*, "A High-Efficiency Broadband Rectenna for Ambient Wireless Energy Harvesting," *IEEE Trans. Antennas Propag.*, vol. 63, 8, pp. 3486–3495, 2015.

[39] ——, "A Novel Six-Band Dual CP Rectenna Using Improved Impedance Matching Technique for Ambient RF Energy Harvesting," *IEEE Trans. Antennas Propag.*, vol. 64, 7, pp. 3160 –3171, 2016.

[40] J. Liang *et al.*, "Study of a printed circular disc monopole antenna for uwb systems," *IEEE Trans. Antennas Propag.*, vol. 53, no. 11, pp. 3500 – 3504, 2005.

[41] H. Sun and W. Geyi, "A New Rectenna With All-Polarization-Receiving Capability for Wireless Power Transmission," *IEEE Antennas Wireless Propag. Lett.*, vol. 15, pp. 814 – 817, 2015.

[42] J. W. Massey and A. E. Yilmaz, "Austinman and austinwoman: High-fidelity, anatomical voxel models developed from the vhp color images," in *2016 38th Annual International Conference of the IEEE Engineering in Medicine and Biology Society (EMBC)*, 2016.

[43] C. Domnik, S. Husges, and C. Degen, "Frugal Energy Harvesting: Microwave Energy Radiated Into the Environment From Wireless Networks," *IEEE Microw. Mag.*, vol. 9, 5, pp. 454 – 462, 2014.

[44] M. Wagih, A. S. Weddell, and S. Beeby, "Characterizing and Modelling Non-Linear Rectifiers for RF Energy Harvesting," in *2019 PowerMEMS*, 2019.

[45] J. Kimionis *et al.*, "Octave and Decade Printed UWB Rectifiers Based on Nonuniform Transmission Lines for Energy Harvesting," *IEEE Trans. Microw. Theory Techn.*, vol. 65, no. 11, pp. 4326 – 4334, 2017.

[46] J. Myers *et al.*, "A Subthreshold ARM Cortex-M0+ Subsystem in 65 nm CMOS for WSN Applications with 14 Power Domains, 10T SRAM, and Integrated Voltage Regulator," *IEEE Journal of Solid-State Circuits*, vol. 51, 1, pp. 31 – 44, 2016.

[47] T. Q. V. Hoang *et al.*, "3D Voltage Pattern Measurement of a 2.45 GHz Rectenna," *IEEE Trans. Antennas Propag.*, vol. 61, 6, pp. 3354 – 3356, 2013.

Mahmoud Wagih (GS'18) received his B.Eng. (Hons.) from the University of Southampton in 2018, where he is currently pursuing his Ph.D.

In 2017, he worked as a Research Assistant at the University of Southampton. In 2018, he was an Engineering Intern, and in 2020, a Research Intern at Arm, Cambridge UK. His research interests are printed and wearable antennas, and rectennas.

Mr. Wagih was the recipient of the Best Undergraduate Project Prize at the University of Southampton, 2018. He was selected for the IEEE IMS Project Connect, 2019. He received the Best Student Paper Award at the IEEE WPTC, 2019, the Best Oral Paper at PowerMEMS 2019, and the Best 3MT (2nd place) at the IEEE Microwave Week, 2020.

Alex S. Weddell (GS'06-M'10) received the M.Eng. degree (Hons.) and Ph.D. in electronic engineering from the University of Southampton, U.K., in 2005 and 2010.

His main research focus is in the areas of energy harvesting and energy management for future Internet of Things devices. He has over 14 years experience in design and deployment of energy harvesting systems, and has published around 55 peer-reviewed papers in the area. He is currently a Lecturer in the Center for Internet of Things and Pervasive Systems at the University of Southampton, and is involved with three projects funded by EPSRC, EU Horizon 2020 and Clean Sky 2.

Steve Beeby received the B.Eng. (Hons.) degree in mechanical engineering from the University of Portsmouth, U.K., in 1992, and the Ph.D. degree from the University of Southampton, Southampton, U.K., in 1998.

He is the Head of the Smart Electronic Materials and Systems Research Group and leads the U.K.'s E-Textiles Network. He is currently leading three U.K. funded research projects and has received over 16 million research funding. He is a Co-Founder of Perpetuum Ltd., a University spin-out based on vibration energy harvesting formed in 2004, Smart Fabric Inks Ltd, and D4 Technology Ltd, Southampton, U.K. He has co-authored/edited four books including Energy Harvesting for Autonomous Systems (Artech House, 2010). He has given 25 invited talks and has over 300 publications and 10 patents. He has an h-Index of 52. His current research interests are energy harvesting, e-textiles, and the use of energy harvesting in wearable applications.

Dr. Beeby was the recipient of two prestigious EPSRC Research Fellowships to investigate the screen-printed materials with micromachined structures for energy harvesting and was awarded a Personal Chair in 2011. He chairs the International Steering Committee for the PowerMEMS Conference series.